Isotopic equilibrium between precipitation and water vapor in Northern Patagonia and its consequences on δ 18 O cellulose estimate

Tiphaine Penchenat, Françoise Vimeux, Valérie Daux, Olivier Cattani, Maximiliano Viale, Ricardo Villalba, Ana Srur, Clément Outrequin

JGR Biogeosciences

RESEARCH ARTICLE
10.1029/2019JG005418

Key Points:
- Each individual rain event deviates from the isotopic equilibrium state with water vapor
- A significant correlation is shown between water vapor isotopic ratios and their expected values at equilibrium with rain over 2 weeks
- A perfect agreement between observed and calculated cellulose isotopic ratio is found when considering the vapor-rain isotopic equilibrium

Supporting Information:
- Data Set S1

Correspondence to:
T. Penchenat,
tiphaine.penchenat@lsce.ipsl.fr

Citation:
Penchenat, T., Vimeux, F., Daux, V., Cattani, O., Viale, M., Villalba, R., et al. (2020). Isotopic equilibrium between precipitation and water vapor in Northern Patagonia and its consequences on $\delta^{18}O_{cellulose}$ estimate. *Journal of Geophysical Research: Biogeosciences*, *125*, e2019JG005418. https://doi.org/10.1029/2019JG005418

Received 5 AUG 2019
Accepted 24 FEB 2020
Accepted article online 25 FEB 2020

Isotopic Equilibrium Between Precipitation and Water Vapor in Northern Patagonia and Its Consequences on $\delta^{18}O_{cellulose}$ Estimate

Tiphaine Penchenat[1], Françoise Vimeux[1,2], Valérie Daux[1], Olivier Cattani[1], Maximiliano Viale[3], Ricardo Villalba[3], Ana Srur[3], and Clément Outrequin[4]

[1]Laboratoire des Sciences du Climat et de l'Environnement (LSCE), Institut Pierre Simon Laplace (IPSL), Gif-sur-Yvette, France, [2]Laboratoire HydroSciences Montpellier (HSM), Institut de Recherche pour le Développement (IRD), Montpellier, France, [3]Instituto Argentino de Nivología, Glaciología y Ciencias Ambientales (IANIGLA), CONICET, Mendoza, Argentina, [4]Centre Européen de Recherche et d'Enseignement des Géosciences de l'Environnement (CEREGE), Aix-en-Provence, France

Abstract Modeling work of the isotopic composition of tree ring cellulose ($\delta^{18}O_{cell}$) relies on the isotopic equilibrium assumption between atmospheric water vapor and tree source water, frequently assimilated to integrated precipitation. Here, we explore the veracity of this assumption based on observations collected during a field campaign in Río Negro province (Argentina) in February–March 2017. We examine how the observed isotopic composition of water vapor deviates from equilibrium with precipitation. This deviation, named isotopic disequilibrium ($\Delta^{18}O_{vap\_eq}$), is low (between −2.0‰ and 4.1‰) and a significant relationship is observed between the isotopic composition of water vapor and its expected value at equilibrium. Negative $\Delta^{18}O_{vap\_eq}$ can be explained by evaporation of small raindrops (from 1% to 5% of initial droplet mass). Positive $\Delta^{18}O_{vap\_eq}$ can result from vegetation transpiration with transpired water accounting for 14% to 29% to ambient water vapor. The low $\Delta^{18}O_{vap\_eq}$ at the study site may be due to the high level of relative humidity (from 70% to 96%) favoring isotopic diffusive exchanges between the two water phases and thus promoting the isotopic equilibrium. We examine the impact of the isotopic equilibrium assumption on the calculation of $\delta^{18}O_{cell}$. A perfect agreement is shown between observed and calculated $\delta^{18}O_{cell}$ provided that the isotopic composition of source water is significantly higher than the expected averaged isotopic composition of precipitation over the tree growing period.

1. Introduction

A number of studies have explored the potential of the width and density of annual tree rings in the Andean mountains of Chile and Argentina to reconstruct past climate variability (e.g., Aravena et al., 2002; Boninsegna et al., 2009; Lara et al., 2005; Mundo et al., 2012; Muñoz et al., 2013; Villalba et al., 1997). Recent studies conducted in the Andean Cordillera between 36°S and 54°S have produced carbon and oxygen series of isotopic composition of tree ring cellulose ($\delta^{13}C$ and $\delta^{18}O$) of various species including *Nothofagus pumilio* (Grießinger et al., 2018; Lavergne et al., 2016; Lavergne et al., 2017; Tognetti et al., 2014), *Austrocedrus chilensis* (Roig et al., 2006), *Fitzroya cupressoides* (Lavergne et al., 2017; Lavergne et al., 2018; Urrutia-Jalabert et al., 2015), and *Araucaria araucana* (Arco Molina et al., 2019). They cover at most the last 200 years. All these studies have evidenced significant links between isotopic records and local climate (temperature, precipitation) and/or patterns of climate variability such as the Southern Annular Mode and El Niño–Southern Oscillation. These strong links indicate that $\delta^{18}O$ and $\delta^{13}C$ of tree ring cellulose represent promising tools for reconstructing past climatic and environmental conditions as well as past atmospheric dynamics in the Southern Hemisphere. Accordingly, additional paleoclimate studies based on the isotopic composition of tree ring cellulose are ongoing in the Andes to reconstruct past climate variations (e.g., in the framework of the THEMES project (The mystery of the expanding Tropics: From past to future).

In order to properly validate the use of the oxygen isotopic composition of tree ring cellulose (hereafter $\delta^{18}O_{cell}$) as a paleoclimate and paleo-environment proxy, the controls on oxygen isotopic fractionation and mixing in the continuum from atmosphere to tree ring cellulose must be known. The $\delta^{18}O_{cell}$ is influenced by a complex mix of climatic and physiological drivers. The $\delta^{18}O$ of atmospheric water vapor

($\delta^{18}O_{vap}$) during the growing season is one of them (Dongmann et al., 1974; Sternberg, 2009; Sternberg et al., 1986; Yakir & DeNiro, 1990). However, prior to the advent of commercial deployable infrared laser-based spectroscopic instruments, measurements of $\delta^{18}O_{vap}$ were difficult: Water vapor had to be trapped cryogenically or with a molecular sieve (Han et al., 2006) and the resulting liquid water equilibrated with CO_2 for isotopic measurement by mass spectrometry. This labor-intensive technique only allowed for off-line determination of $\delta^{18}O_{vap}$ with a low temporal resolution. As a consequence, $\delta^{18}O_{vap}$ data were rare and vapor was considered in isotopic equilibrium with source water in studies devoted to the modeling of oxygen isotopic composition in leaves and rings (Cernusak et al., 2016; Sternberg, 2009).

With deployable infrared laser-based instruments, $\delta^{18}O_{vap}$ can be directly measured at a high time resolution and the water vapor-rain assumption can now be checked. In this paper, we examine, for the first time in southern South America, the validity of the isotopic equilibrium between precipitation and water vapor. For this purpose, a field campaign was organized in the western part of the Río Negro, Patagonian Andes, Argentina, as part of the IVAPAPA project (Isotopes dans la Vapeur, les Pluies et les Arbres de Patagonie) to provide isotopic observations in both water vapor and rain. These data will be exploited in particular in the ongoing THEMES project mentioned above.

2. Data and Methods

2.1. Description of the Survey Site

The field campaign took place from 24 February to 26 March 2017 in the Andean Cordillera, at a site located at about 20 km north of the city of El Bolson and 17 km east of the Chilean border, in the province of Río Negro, Argentina (41°47.412′S, 71°34.355′W, 1,175 m) (Figures 1a–1c). The site is located on the eastern leeward side of the Andes. Humid air masses from the Pacific generate precipitation through orographic uplift when the dominant Westerly winds encounter the Andes mountain (Garreaud et al., 2013). The resulting west-to-east humidity gradient is accentuated by downslope winds (Seluchi et al., 2003). At ~41°S, annual precipitation reaches 2,050 mm/year on the west side of the Andes (at Calbuco, see Climate-data.org), whereas it is about half this amount 120 km to the East (1,036 mm/year at El Bolson). This decrease is accompanied by a steep vegetation gradient from temperate rainforest on the Pacific side to mesic *Nothofagus* forest in the rain shadow slopes.

The investigated site is at the Cerro Perito Moreno ski station. It is located ~80 km south from Lavergne et al.'s (Lavergne et al., 2016; Lavergne et al., 2017; Lavergne et al., 2018) sampling sites. This site was selected because (1) it is far from lakes and thus likely not affected by local moisture sources and (2) it is surrounded by a forest of *Nothofagus pumilio* trees and located close to the tree line, presenting similar environmental conditions to those of the sites studied in the aforementioned Lavergne et al.'s studies. Practical reasons were also decisive in choosing the site: The ski station is easily accessible by road and it provides a shelter and reliable power supply, facilities not available on Lavergne et al.'s (Lavergne et al., 2016; Lavergne et al., 2017; Lavergne et al., 2018) sites. In consequence, we were able to test the isotopic equilibrium hypothesis in a similar environment with the same species as those investigated by Lavergne et al. (2016; 2017; 2018).

2.2. Meteorological Data Used During the Field Campaign

In this study, we used different meteorological data sets. First, a data logger (HOBO® sensor from Onset Computer Corp) was set up on site. It recorded temperature (T_{air}) and relative humidity (rh) from 24 February to 31 March 2017 at a few meters from the ground, with a 5-min time resolution. Local precipitation was collected by a classical rain gauge (cone-shaped SPIEA model 1650-02) located 10 m far from the refuge (Figure 1c).

We also used meteorological data from three remote stations: Pampa Linda (41°13′50″S, 71°46′21″W, 65 km north of the study site), La Balza (43°21′39″S, 72°3′56″W, 154 km south of the study site), and Trevelin (43°5′33″S, 71°24′26″W, 146 km south of the study site) (Figure 1a). Hourly mean precipitation data are available from 1 January to 30 April 2017 at La Balza and Trevelin and from 25 November 2016 to 31 December 2017 at Pampa Linda.

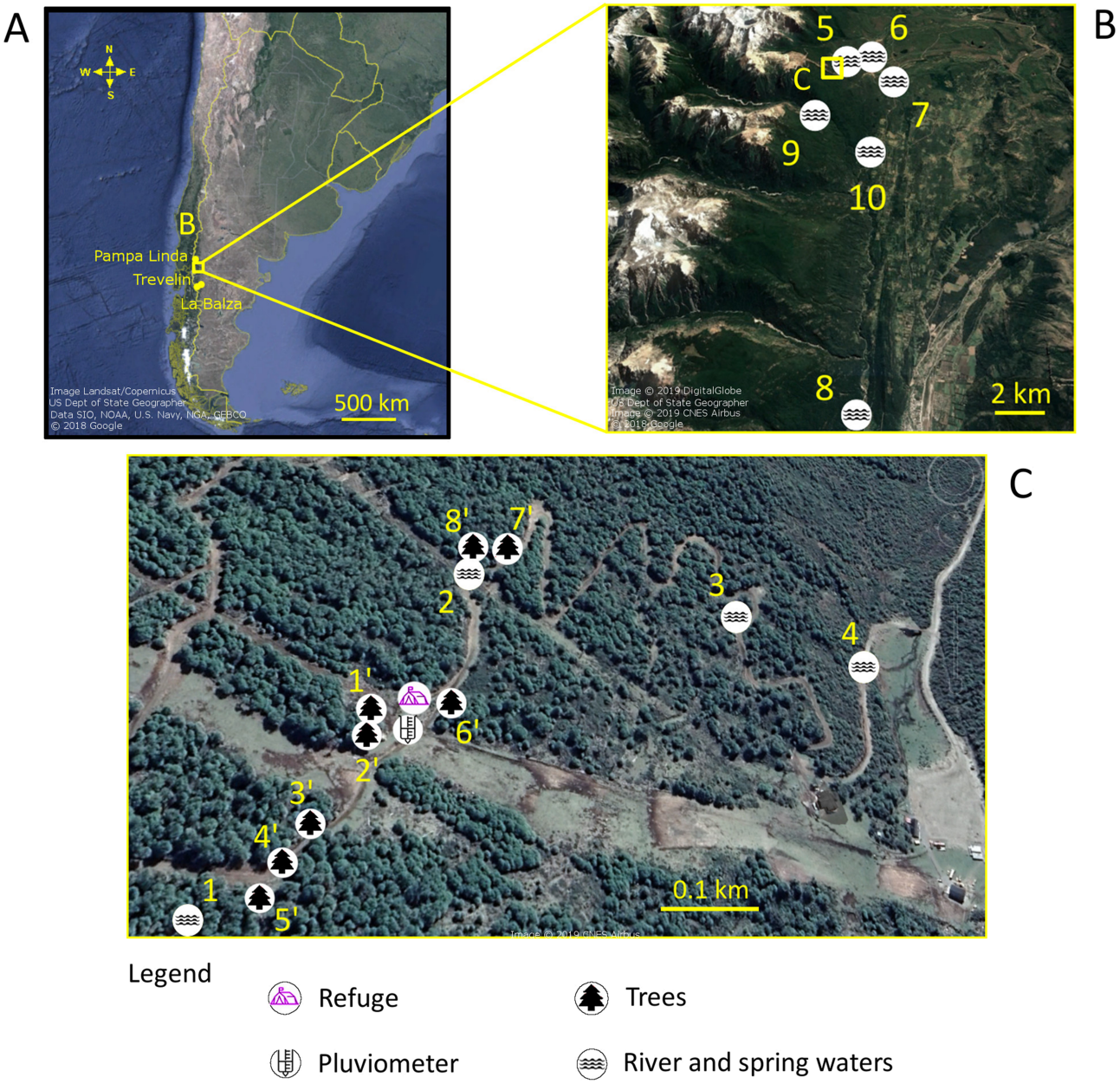

Figure 1. (a) Location of the survey site in Argentina (yellow box); (b) Zoom of the B box shown on Figure 1a showing the locations of river and spring samples (Samples 5 to 10); (c) Zoom of the C box shown on Figure 1b showing the location of other river and spring samples (1 to 4), tree core samples (2′, 3′, 4′, 5′, and 8′), leaf samples (1′, 3′, 4′, 6′, 7′, and 8′), the pluviometer and the refuge where the Picarro® instrument was installed. Google Earth (12 February 2019). Argentina. 41°47.412′S, 71°34.355′W, Eye alt 4,757 feet. SIO, NOAA, U.S. Navy, NGA, GEBCO. Images Landsat/Copernicus, DigitalGlobes 2019, CNES Airbus 2019, U.S. Department of State Geographer (https://earth.google.com/web/) [February, 2019].

2.3. Water Vapor Measurements

Water vapor mixing ratio (q_{vap}) and the isotopic composition of the water vapor ($\delta^{18}O_{vap}$ and $\delta^{2}H_{vap}$) were measured by a laser instrument (Picarro®, L2130-i), based on the wavelength-scanned cavity ring down spectroscopy and set up in an isolated room to reduce temperature fluctuations (Figure 1c). The instrument was operational from 24 February at 17:07 UTC to 26 March 2017 at 11:57 UTC. Our experimental setup was similar to the one described in Tremoy et al. (2011). In short, water vapor was captured at about 5 m high through a heated intake of 10 m long and 3/8 inch diameter tubing (perfluoroalkoxy, PFA). The sample line was pumped at ~0.6 L/min. As described in Tremoy et al. (2011), q_{vap} was calibrated against a HOBO sensor

(measuring temperature and relative humidity) on site from 24 February 17:05 UTC to 26 March 11:55 UTC. Corrections were applied to account for the dependence on humidity of the isotopic composition and to eliminate the isotopic instrumental drift, following the protocol described in Tremoy et al. (2011). Both corrections were determined using the Standard Module Delivery (SDM) from Picarro Inc. The first correction was assessed by injecting two water standards at different humidity levels from ~1,000 to ~18,500 ppm. The isotopic calibration of the instrument was performed every 24 hr based on the injection of two standards at a reference water vapor concentration of ~14,000 ppm. The short-term precision of the instrument ($\pm 1\sigma$) during a 10-min stable measurement of water standard was better than ±0.2‰ and ±0.7‰ for $\delta^{18}O_{vap}$ and $\delta^{2}H_{vap}$, respectively, leading to a precision better than ±1.8‰ for deuterium excess ($d_{vap} = \delta^{2}H_{vap} - 8 \times \delta^{18}O_{vap}$, Dansgaard (1964)).

2.4. Precipitation Sampling and Measurements

During the field campaign, we collected 11 precipitation events (R1 to R11) between 27 February and 12 March 2017 (no rain occurred before and after these dates during the field campaign). The isotopic composition of precipitation ($\delta^{2}H_{prec}$ and $\delta^{18}O_{prec}$) was analyzed using an infrared-based laser instrument (Picarro®) for $\delta^{2}H$ and CO_2-H_2O equilibration coupled to a mass spectrometer (Finnigan MAT 252) for $\delta^{18}O$. The uncertainties were ±0.7‰ and ±0.05‰ for $\delta^{2}H$ and $\delta^{18}O$, respectively, leading to an uncertainty of ±0.8‰ for deuterium excess.

Precipitation in the rain gauge was collected only when the observer was in the field. As a consequence, the rain hours were not known precisely and each rain sample covered a different time period noted P (P1 to P11). The duration of P periods was around 23 hr, except for two P periods due to field constraints: 1 hr and 15 min for P8 and 45 hr for P5. It is worth noting that only P11 recorded a mixing between snow and rain. Although we did not know the partition between the two water phases, surface temperature was always higher than 5 °C, which was rather in favor of a larger proportion of rain relative to snow.

Within the P periods, the start and end times of each rain event had to be estimated. First, an abrupt rh increase (>10%/hr, arbitrary fixed) up to saturation was considered as a marker of the beginning of the rain. However, as rh displayed a diurnal cycle (Figure S1 in the supporting information) with a minimum between 20:00 UTC and 23:00 UTC, an abrupt increase of rh during this time window may have been undetected. In addition, during some P periods, rh did not exhibit any abrupt increase. Comparison of the precipitation records at La Balza, Trevelin, and Pampa Linda revealed consistency in occurrence and time of rain events in 86% of the cases from 25 February to 15 March 2017 (384 hr) (Figure S2). We took advantage of this regional rain pattern to deduce the start and end time of rain events at our study site from those at Pampa Linda (the closest station) when local rh could not be used. When Pampa Linda rain hours were used for the determination of rain events at our site, we checked that rh on our site was high enough to be consistent with a period of rain. The estimated rain periods after applying the aforementioned methodology were noted R1 to R11 (see details in the supporting information in Figures S3–S13 and in Table S1).

2.5. River Water Samples

Seven local river and spring waters were also sampled in the area of the shelter (within 2 km) on 25 February 2017 (Figure 1c). Three additional samples were taken south of our site, along the Rio Azul, on 25 February 2017 (Sample 8, 18 km south) and 22 March 2017 (Samples 9 and 10, 5.5 km and 3 km south, respectively) (Figure 1b). The isotopic composition ($\delta^{18}O$ and $\delta^{2}H$) of those samples was analyzed with the same methodology as for precipitation, leading to similar uncertainties (see section 2.4).

2.6. Leaf Water and Cellulose Samples

Because of logistic difficulties, we were not able to sample xylem water during the field campaign. However, we sampled some *Nothofagus* leaves to measure the isotopic composition of their water. Leaves were sampled on six hand-reach trees on 25 March 2017 between 15:35 and 16:50 UTC (Figure 1c).

Leaf water was extracted with a vacuum distillation line (Alexandre et al., 2018). To measure the $\delta^{18}O$ of leaf water in the laboratory with a mass spectrometer (Finnigan MAT 252), we used the fluorination methodology following Barkan and Luz (2005) to separate oxygen from hydrogen. It is worth noting that we extracted the water from the whole leaves, without differentiating enriched water from the evaporation site from depleted water from the veins. The uncertainty was ±0.05‰.

The oxygen isotopic composition of the cellulose of the 2016–2017 ring from five *Nothofagus* trees ($\delta^{18}O_{cell\text{-}mes}$) growing in the Cerro Perito Moreno site was determined following the procedure described in Lavergne et al. (2016) (Figure 1c). The wood samples were chipped and then grounded in a ball mill for homogenization. Alpha-cellulose was extracted from the wood following the SOXHLET chemical method derived from Leavitt and Danzer (1993) and then homogenized ultrasonically with a sonotrode apparatus and freeze-dried. Cellulose samples of around 0.2 mg were loaded in silver foil capsules. The $\delta^{18}O_{cell}$ was obtained with a high temperature conversion elemental analyzers (TC-EA, Thermo Scientific for oxygen) coupled with a mass spectrometer (IRMS IsoPrime. The uncertainty was ±0.2‰).

2.7. Definition of the Isotopic Disequilibrium

In this paper, the isotopic disequilibrium is defined as the difference between the measured $\delta^{18}O_{vap}$ (‰) and the calculated isotopic composition of vapor at equilibrium with the rain ($\delta^{18}O_{vap\_eq}$, ‰):

$$\Delta^{18}O_{vap\_eq} = \delta^{18}O_{vap} - \delta^{18}O_{vap\_eq} \tag{1}$$

where

$$\delta^{18}O_{vap} = \frac{\left({}^{18}O\,/{}^{16}O\right)_{\text{vapor sample}}}{\left({}^{18}O\,/{}^{16}O\right)_{\text{VSMOW}}} - 1, \tag{2}$$

where VSMOW is the international standard (Standard Mean Ocean Water).

And $\delta^{18}O_{vap\_eq}$ is calculated according to

$$\delta^{18}O_{vap\_eq} = \frac{\delta^{18}O_{prec} + 1}{\alpha_{eq}} - 1, \tag{3}$$

where α_{eq} (>1) is the precipitation-water vapor equilibrium fractionation coefficient for oxygen. It is calculated from the equation given in Majoube (1971) using the air surface temperature averaged over precipitation events.

The disequilibrium can also be defined as the difference between the measured $\delta^{18}O_{prec}$ and the isotopic composition of precipitation in equilibrium with water vapor ($\delta^{18}O_{prec\_eq}$):

$$\Delta^{18}O_{prec\_eq} = \delta^{18}O_{prec} - \delta^{18}O_{prec\_eq} \tag{4}$$

Using $\Delta^{18}O_{vap\_eq}$ or $\Delta^{18}O_{prec\_eq}$ for investigating the isotopic equilibrium is of no consequence in our study. Actually, our discussion will be based on the sign of $\Delta^{18}O_{vap\_eq}$. In our observations, a positive $\Delta^{18}O_{vap\_eq}$ implies a negative $\Delta^{18}O_{prec\_eq}$ and conversely (see section 3.2). So, the two approaches are symmetrical and lead to the same conclusions. However, we will refer to $\Delta^{18}O_{prec\_eq}$ in addition to $\Delta^{18}O_{vap\_eq}$ to constrain further the influence of droplets evaporation on isotopic equilibrium (section 4.1.1.1). It is also worth noting that the use of deuterium instead of oxygen 18 to quantify the isotopic disequilibrium leads to similar results and conclusions.

A positive $\Delta^{18}O_{vap\_eq}$ (respectively negative $\Delta^{18}O_{prec\_eq}$) means that the isotopic composition of water vapor is higher than (respectively that the isotopic composition of precipitation is lower than) what would be expected at isotopic equilibrium.

3. Results

3.1. Observations

Raw observations are reported in Figure 2. The mean air temperature (T_{air}) over the data set was 11.4 ± 5.6 °C with a maximum of 28.5 °C and a minimum of 0.8 °C. The mean rh was 66 ± 16% with a maximum of 97% and a minimum of 22%. The mean, maximum, and minimum mixing ratio q_{vap} were 6.3 ± 1.7, 12.7, and 2.3 g/kg, respectively.

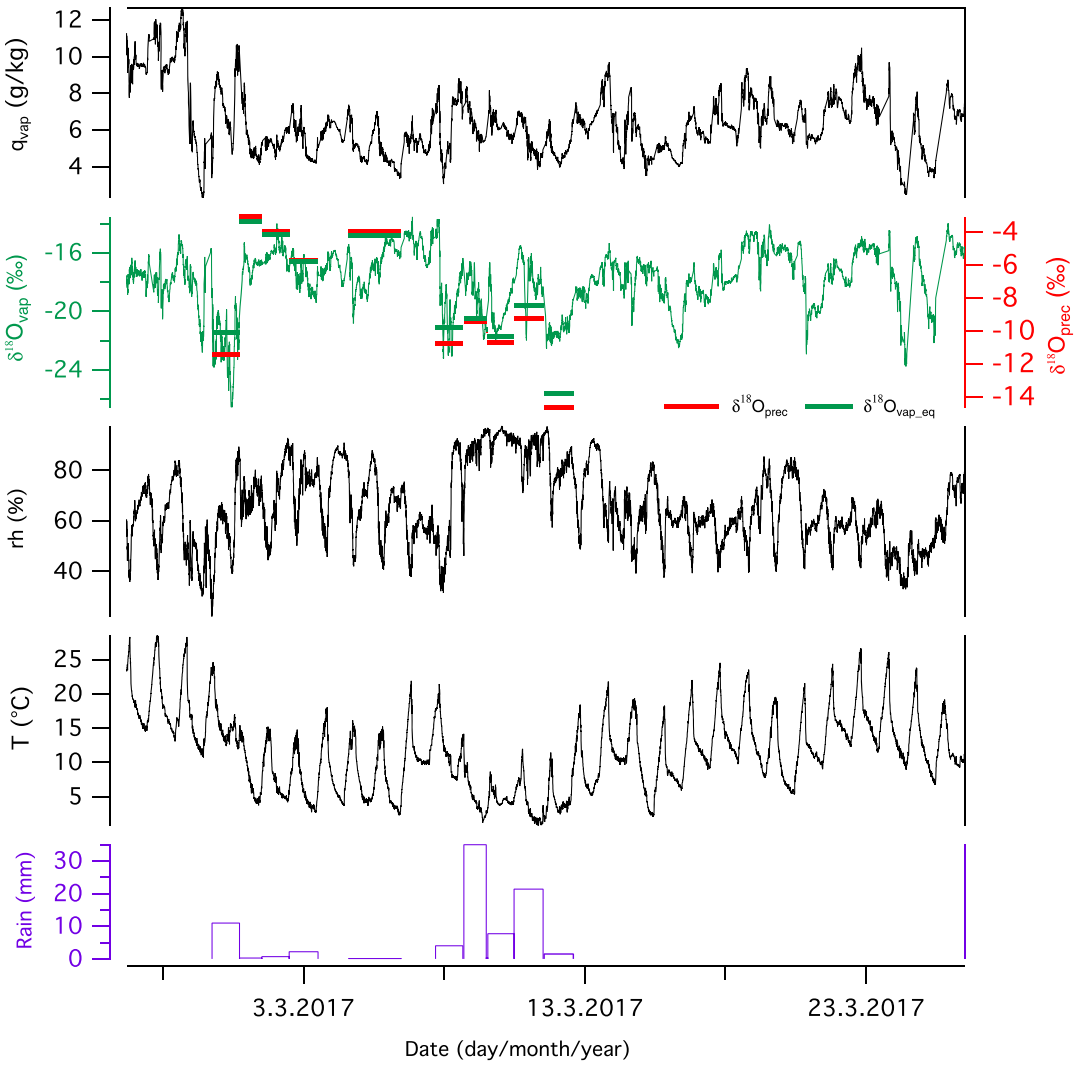

Figure 2. From top to bottom, temporal evolution of q_{vap} (g/kg), $\delta^{18}O_{vap}$ (‰) (water vapor isotopic scale is on the left green axis), rh (%), temperature (°C), and total amount of precipitation (mm) for each *P* periods from 24 February 2017 at 17:05 UTC to 26 March 2017 at 12:00 UTC. The red dashes correspond to the isotopic composition of the rain events ($\delta^{18}O_{prec}$, ‰, right red axis), and the green dashes correspond to the isotopic composition of water vapor at equilibrium with the rainwater ($\delta^{18}O_{vap\_eq}$, ‰, left green axis).

Over the whole period, T_{air}, rh, and q_{vap} exhibited a clear diurnal cycle with an amplitude of 10.5 °C (from 7.5 to 18.3 °C), 23% (from 51% to 74%), and 2.2 g/kg (from 5.5 to 7.7 g/kg), respectively. There was a period with conditions close to saturation (rh varied from 82.4% to 97.6%) between 8 March at 18:00 UTC and 11 March at 14:45 UTC with an attenuated diurnal cycle. The air temperature, ranging from 0.9 to 11.5 °C, was low during this period. This period was also rainy: Six rain events occurred representing 69.6 mm of rainwater (i.e., 83% of the total rainwater collected during the field campaign).

$\delta^{18}O_{vap}$ varied significantly with a maximum of −13.6‰ and a minimum of −26.5‰. The mean $\delta^{18}O_{vap}$ value was −17.8 ± 2.1‰. A clear diurnal cycle appeared (this is illustrated on Figure S1) with a mean amplitude of 2.2‰ (from −18.8‰ to −16.6‰, subseasonal variations not removed). $\delta^{18}O_{prec}$ was very different from one rain event to another and ranged between −3.1‰ and −14.6‰ with an amount-weighted average of −9.7 ± 2.9‰.

3.2. Calculation of the Isotopic Disequilibriums

Isotopic disequilibrium was not calculated for rain events R2 and R8 because they occurred during the daily isotopic calibration of the instrument (see section 2.3); therefore, water vapor data could not be collected. For

Table 1
$\Delta^{18}O_{vap\_eq}$ and $\Delta^{18}O_{prec\_eq}$ (‰) Calculated for Each R and P Event and Differences Between $hem

	$\Delta^{18}O_{vap\_eq}$ (‰)			$\Delta^{18}O_{prec\_eq}$ (‰)		
N°	P	R	P-R	P	R	P-R
1	−1.0	−0.5	−0.5	1.0	0.5	0.5
2	−3.0			3.0		
3	−1.3	−2.0	0.7	1.3	2.0	−0.7
4	−1.2	−1.0	−0.2	1.2	1.0	0.2
5	−2.2	−2.0	−0.3	2.2	2.0	0.3
6	2.1	1.8	0.3	−2.1	−1.8	−0.3
7	1.4	1.4	0.0	−1.4	−1.4	0.0
8						
9	1.9	1.3	0.5	−2.0	−1.3	−0.5
10	1.9	2.3	−0.4	−2.7	−2.3	−0.4
11	4.4	4.1	0.3	−4.4	−4.2	−0.3
Mean (‰)	0.3	0.6	0.1	−0.4	−0.6	−0.1
σ (‰)	2.3	2.1	0.4	2.4	2.1	0.4

the other nine R events, the calculation of $\Delta^{18}O_{vap\_eq}$ was performed using $\delta^{18}O_{vap}$ data averaged over the length of each rain event (Table 2).

We defined the start and the end times of rain events as precisely as possible. As shown in Table 2, isotopic disequilibriums calculated over the R events were not significantly different from those calculated over the P periods. The differences in $\Delta^{18}O_{vap\_eq}$ between R events and P time periods ranged from −0.5‰ to +0.7‰ with a mean not significantly different from zero (0.1 ± 0.4‰). In the following, we only discuss isotopic disequilibriums calculated over the R events.

It is worth mentioning that $\Delta^{18}O_{vap\_eq}$ are means over the R events. However, we know that rain does not occur at a consistent rate during any one event. So, ideally, the disequilibrium calculation would take this into account. Practical limitations on the field regarding the rain sampling prevent doing this in our study although the temporal resolution of laser-based measurements would allow it. In addition, in case local precipitation rate evolution is known along the rain event, one should also consider using a precipitation amount-weighted average $\delta^{18}O_{vap}$ over the rain event. This temporal offset may explain some component of $\Delta^{18}O_{vap\_eq}$.

$\Delta^{18}O_{vap\_eq}$ varied between −2.0 and 4.1‰ (Table 1; Figure 3). The highest $\Delta^{18}O_{vap\_eq}$ (4.1‰) occurred for the R11 event, which corresponded to a mixing of rain and snow. From R1 to R5, $\Delta^{18}O_{vap\_eq}$ were negative (processes caused a depletion of the vapor with respect to equilibrium), whereas they were positive from R6 to R11 (processes enriched the vapor with respect to equilibrium).

Interestingly, $\Delta^{18}O_{vap\_eq}$ were negatively correlated to $\delta^{18}O_{prec}$ with r^2 of 0.75 ($n = 9$) (Figure 4). As $\delta^{18}O_{prec}$ decreased, $\Delta^{18}O_{vap\_eq}$ increased and became positive. This means that processes responsible for the isotopic disequilibrium could also control $\delta^{18}O_{prec}$ (no specificity for R1 event can explain its deviation from the linear regression).

We also noted that the covariation of $\delta^{18}O_{vap}$ and $\delta^{18}O_{vap\_eq}$ was highly significant ($r^2 = 0.78$, $n = 9$).

4. Discussion

4.1. Processes Involved in the Isotopic Disequilibriums

In the following sections, we discuss the different processes that can induce a departure from the isotopic equilibrium between water vapor and precipitation. We assume that water vapor and precipitation are initially at the isotopic equilibrium. We simplify the discussion by exploring processes moving the two water phases away from equilibrium one by one (in real conditions, it is very likely that several processes occur at the same time or sequentially).

Our discussion is organized in two sections. First, we discuss processes that could lead to $\Delta^{18}O_{vap\_eq} < 0$ and consistent with high $\delta^{18}O_{prec}$, namely, (i) the evaporation of raindrops during their fall and (ii) the evaporation of soil water. Second, we discuss processes leading to $\Delta^{18}O_{vap\_eq} > 0$ and consistent with low $\delta^{18}O_{prec}$, namely, (i) the condensation of water vapor at very high altitude, (ii) the size of droplets, and (iii) the transpiration from vegetation.

4.1.1. Case 1: $\Delta^{18}O_{vap\_eq} < 0$ (and $\Delta^{18}O_{prec\_eq} > 0$)

The processes discussed in this section tend to deplete water vapor and to enrich precipitation relative to the isotopic equilibrium. They are involved in the R1 to R5 events.

4.1.1.1. Evaporation of Raindrops During Their Fall

When evaporation of droplets occur in unsaturated environment, the isotopic composition of both phases evolves following the Stewart's theory (1975) (also described in Bony et al., 2008). This theory treats evaporation and diffusive processes in a uniform manner and describes the evolution of $\delta^{18}O_{prec}$, $\delta^{18}O_{vap}$, d_{vap}, and d_{prec} during the evaporation as a function of the residual water fraction noted f (at $f = 1$ no evaporation occurs and at $f = 0$ droplet is fully evaporated). In our study, we hypothesize that the initial state ($f = 1$) is the isotopic equilibrium so that $\delta^{18}O_{prec}$ ($f = 1$) = $\delta^{18}O_{prec\_eq}$ and $\delta^{18}O_{vap}$ ($f = 1$) = $\delta^{18}O_{vap\_eq}$.

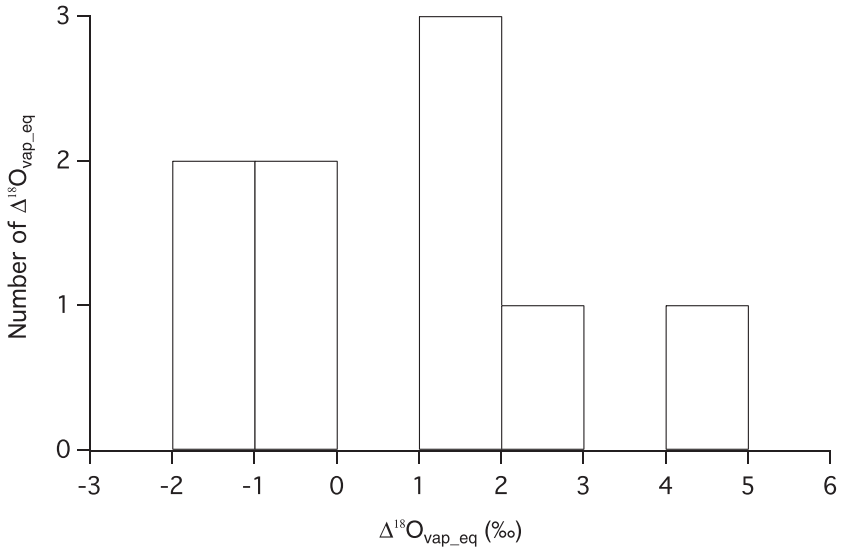

Figure 3. Distribution of $\Delta^{18}O_{vap\_eq}$ (‰).

Figure 5a (and Figure S14a) shows that the evaporation of droplets always induces an increase of $\delta^{18}O_{prec}$ and thus leads to a positive $\Delta^{18}O_{prec\_eq}$. As evaporation proceeds, the surrounding water vapor gets enriched (in the limit case where all the rain is evaporated, the vapor isotopic composition is the weighted mean between the compositions of the original vapor and rain. This composition is richer than the original vapor composition since the condensate is always richer than the vapor) and $\Delta^{18}O_{vap\_eq}$ turns to be positive as f approaches to 0 (Figure 5a). However, for small evaporation fraction ($f > 0.91$ in Figure 5a), $\delta^{18}O_{vap}$ slightly decreases compared to the equilibrium value and $\Delta^{18}O_{vap\_eq}$ is negative ($\delta^{18}O_{vap\_obs} < \delta^{18}O_{vap\_eq}$).

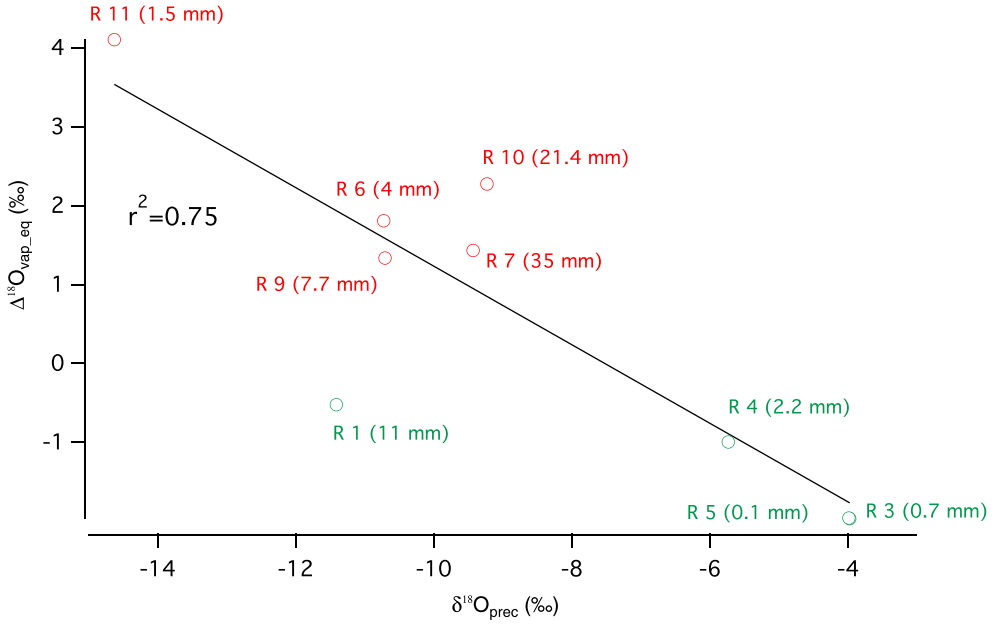

Figure 4. $\Delta^{18}O_{vap\_eq}$ (‰) as a function of $\delta^{18}O_{prec}$ (‰) for each R event (except for R2 and R8 when $\delta^{18}O_{vap}$ was not recorded). The covariation coefficient is $r^2 = 0.75$. Green (red) circles correspond to negative (positive) water vapor disequilibriums. Observations corresponding to R3 and R5 are so close that they cannot be distinguished on this figure.

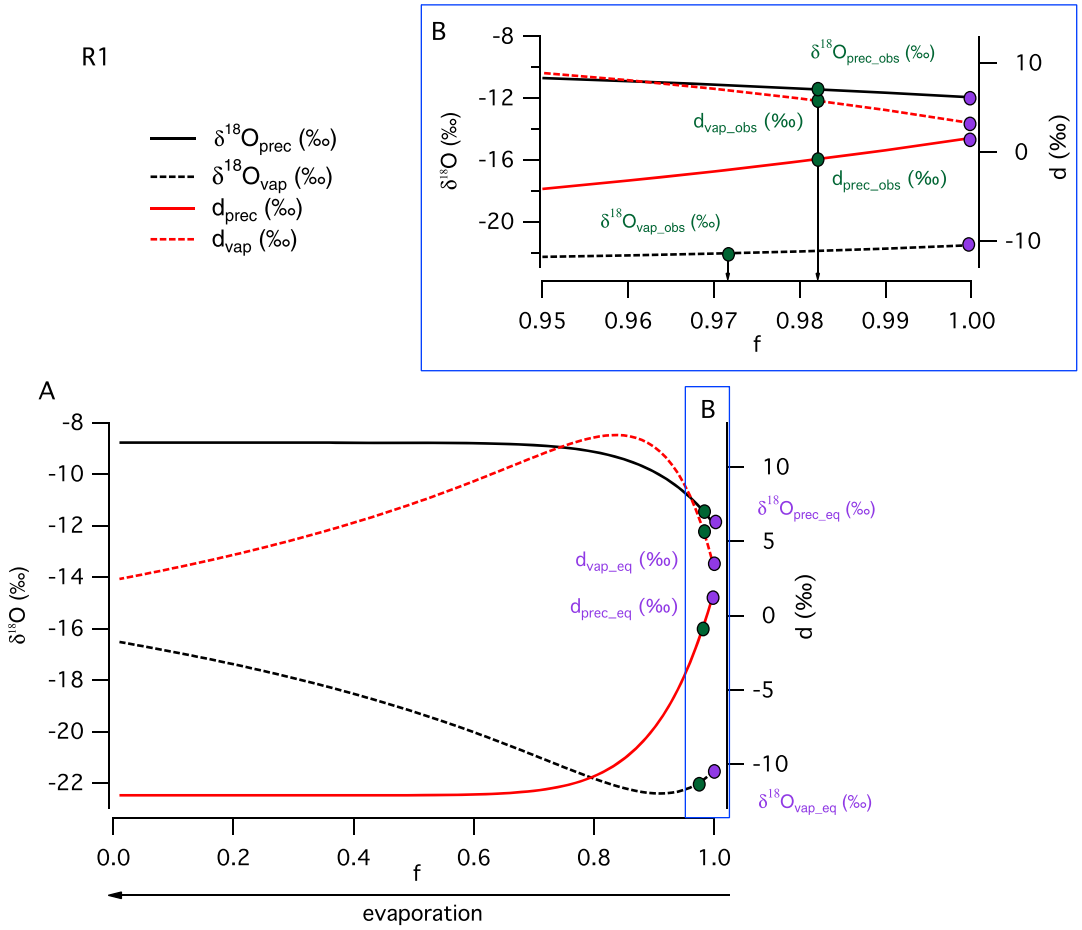

Figure 5. (a) Evolution of the isotopic composition of water vapor (dashed line) and precipitation (solid line) during reevaporation of a droplet as a function of the residual droplet fraction f ($f = 0$, no more droplets; $f = 1$, no evaporation) for $\delta^{18}O$ (black curves) and for deuterium excess (red curves) during R1 event, following the theory of Stewart (1975) and Bony et al. (2008). Purple circles are the isotopic composition of water vapor ($\delta^{18}O_{vap\_eq}$ and d_{vap_eq}) and precipitation ($\delta^{18}O_{prec\_eq}$ and d_{prec_eq}) in equilibrium with observed precipitation and water vapor, respectively. Green circles are the observed isotopic composition of water vapor ($\delta^{18}O_{vap\_obs}$ and d_{vap_obs}) and precipitation ($\delta^{18}O_{prec\_obs}$ and d_{prec_obs}); (b) Zoom of panel (a) picture for f varying between 0.95 and 1. The black arrows indicate the fraction of evaporation deduced from observations. It is here of 1% to 5%. See Figure S14 in the supporting information for R4 event.

Therefore, for R1 to R5, if droplet evaporation is the only process responsible for the isotopic disequilibrium (which is discussed below), the $\Delta^{18}O_{vap\_eq} < 0$ condition would indicate that the evaporated fraction is very small (i.e., f close to 1). Figure 5a also shows the evolution of the deuterium excess in both phases. As evaporation proceeds, d_{prec} decreases whereas d_{vap} first increases and then decreases to attain a final value (at $f = 0$) slightly higher than the initial value. As a consequence, evaporation processes cannot be involved in R events exhibiting $d_{prec} > d_{prec\_eq}$ which is the case for R3 ($d_{prec} = 14.8‰$ and $d_{prec\_eq} = 12.9‰$) and R5 ($d_{prec} = 11.5‰$ and $d_{prec\_eq} = 9.4‰$).

In order to quantify the evaporated fractions corresponding to our observations, the isotopic composition for R1 and R4 are plotted on Figures 5 and S14, respectively. In such diagrams, the evaporated fraction ($1 - f$) is given by the intercept between observations and theoretical curves. For water vapor, the evolution of the isotopic composition as a function of f is nonmonotonic and two solutions can be found for both δ and d. The one consistent with the precipitation curves ($\delta^{18}O$ and d) has to be chosen.

The evaporation rates of droplets for the R1 and R4 events are between 1% and 5% (Figures 5b and S14b). The obtained evaporation fractions for our observations are very low in comparison to evaporation rates close to

60%, which can be reached in some convective regions (Tremoy et al., 2014). They are nonetheless sufficient to explain the small observed isotopic disequilibriums. It is worth noting that during the R1 and R4 events, rh was of 70% and 73%, respectively, among the lowest rh values recorded during the campaign. The hypothesis of droplets evaporation is consistent with the relatively high $\delta^{18}O_{prec}$ values measured for R1 and R4 (Figure 4) as evaporation increases the isotopic composition of precipitation.

4.1.1.2. Evaporation of Soil Water

Evaporation of surface soil water, which may generate a very depleted flux toward the atmosphere, can induce a depletion of the isotopic composition of water vapor relative to the isotopic equilibrium. To calculate the isotopic composition of the evaporative flux from the soil, the simplified equation from Craig and Gordon (1965) is used:

$$\delta_{ev\_flux} = \frac{\delta_{soil} - rh \times \delta_{vap} + \varepsilon_{v-1} + \varepsilon_{diff}}{1 - rh} \quad (5)$$

Where δ_{soil} and δ_{vap} are the oxygen or deuterium isotopic compositions of soil water and water vapor, respectively, rh is the relative humidity of the air, ε_{v-1} is the equilibrium fractionation parameter defined as

$$\varepsilon_{v-1} = \left(\left(\frac{1}{\alpha_{eq}}\right) - 1\right) \times 1000, \quad (6)$$

and ε_{diff} is the kinetic fractionation parameter defined as

$$\varepsilon_{diff} = \left((1 - rh) \times \left(1 - \frac{D}{D^*}\right)^n\right) \times 1000. \quad (7)$$

Where D/D* is the ratio of molecular diffusivities in air of the most ($H_2{}^{16}O$) and less ($H_2{}^{18}O$ or $HD^{16}O$) abundant isotopologues (1.0285 and 1.0251 for $H_2{}^{18}O$ and $HD^{16}O$, respectively) (Merlivat, 1978), and *n* is a turbulence parameter linked to the surface roughness. According to Brutsaert (1982), this exponent depends on the air water content of the atmosphere and varies between 0.5 (turbulent flow), 2/3 (laminar flow), and 1 (molecular diffusion). In a number of studies (Barnes & Allison, 1983, 1984, 1988; Mathieu & Bariac, 1996) the value $n = 1$ is used. However, as mentioned in both Braud et al. (Braud, Bariac et al., 2009; Braud, Biron et al., 2009) and Rothfuss et al. (2015) studies, *n* was observed to vary in time and between evaporation stages. As a consequence, we experiment here the three values of *n* in our calculations as already done in Braud et al. (Braud, Biron et al., 2005; Braud, Bariac et al., 2005).

Then, we define what the contribution of evaporated soil water to the near-surface water vapor should be to explain the deviation of the observations from the equilibrium state. This contribution (*x*) is given by

$$\delta_{vap} = x \times \delta_{ev\_flux} + (1 - x) \times \delta_{vap\_eq} \quad (8)$$

So that *x* is equal to:

$$x = \left(\frac{\delta_{vap} - \delta_{vap\_eq}}{\delta_{ev\_flux} - \delta_{vap\_eq}}\right) \quad (9)$$

The isotopic composition of soil water is usually affected by evaporation from the surface down to ~30 cm at the most (evaporation front, see, e.g., Sprenger et al., 2016, for a recent review). Therefore, we considered here that water below the evaporation front is isotopically close to that of rivers and springs (although rivers and springs may derive partially from rain and snow infiltrated at higher elevation, see section 4.2) and representative of long-term rainfall, as it is frequently the case (Darling, 2004; Halder et al., 2015; Saylor et al., 2009). The isotopic composition of the subsoil water, below the evaporation front, thus equals the mean value of the isotopic composition of river and spring samples ($\delta^{18}O_{river} = -11.5 \pm 0.5‰$ and $\delta^{2}H_{river} = -84.2 \pm 4.9‰$). The value of *x* is calculated assuming that the soil water (above the evaporation front and thus enriched by evaporative processes compared to the subsoil water) has a $\delta^{18}O_{soil}$ between −11‰ and −3‰ (with a $\delta^{2}H_{soil}$ in a ratio of 5 to $\delta^{18}O_{soil}$ according to Sprenger et al. (2016), that is,

Table 2
Contribution of the Tree Transpiration (%) Calculated for $\delta^{18}O$ and $\delta^{2}H$ Disequilibriums for R6 to R11 (Except R8). $\delta^{18}O_{soil}$ and $\delta\ ^{2}H_{soil}$ Used in the Calculation Are the Mean Isotopic Compositions of River Samples

	Contribution (%)	
Events	$\delta^{18}O$	$\delta^{2}H$
R6	19	24
R7	16	14
R9	13	15
R10	25	26
R11	29	28

between −55‰ and −15‰) and using different values for n in equation 7. Whatever the composition of the soil water considered, the calculated contributions x for $\delta^{18}O$ and $\delta^{2}H$ are inconsistent with each other and can be even negative or superior to 1 for the highest values of $\delta^{18}O_{soil}$.

As a conclusion, soil water evaporation cannot explain any of the observed disequilibrium during our field campaign.

4.1.2. Case 2: $\Delta^{18}O_{vap\_eq} > 0$ and $\Delta^{18}O_{prec\_eq} < 0$

In this section, we discuss positive disequilibriums. The involved processes enrich the vapor and deplete the precipitation relative to the isotopic equilibrium. They are involved in the R6 to R11 events.

4.1.2.1. Formation of Raindrops at Very High Altitude

The isotopic composition of water vapor decreases with altitude (Dansgaard, 1964). Thus, raindrops formed at high elevation exhibit isotopic compositions lower than the value corresponding to the isotopic equilibrium with surface water vapor. If exchanges between droplets and water vapor are reduced during rainfall, for example, during strong storms, the higher the altitude of condensation, the larger the distance to isotopic equilibrium. When such disequilibrium occurs, $\delta^{18}O_{prec}$ is lower than $\delta^{18}O_{prec\_eq}$ inducing a positive $\Delta^{18}O_{vap\_eq}$.

If this process is at play, $\Delta^{18}O_{vap\_eq}$ is all the higher as the rain is formed at high altitude and therefore as $\delta^{18}O_{prec}$ is depleted, consistent with the correlation exhibited in Figure 4. However, as we do not have information on condensation elevation, we cannot quantify the impact of this process in our study.

4.1.2.2. Formation of Large Drops of Water

A raindrop falls through an environment more and more enriched relative to the vapor it was formed from. Therefore, the exposure of the drop to its environment has to be taken into account. We speculate that small and slow raindrops come to a more complete isotopic equilibrium with surrounding water vapor than large and fast falling raindrops produced by convective events. In our observations, the largest positive disequilibriums occur with highly depleted precipitation (Figure 4). This could reflect the presence of big storms producing large and relatively depleted drops and preventing rain and water vapor to equilibrate during drop fall. In that case, $\delta^{18}O_{prec}$ would be more negative than $\delta^{18}O_{prec\_eq}$ leading to a positive $\Delta^{18}O_{vap\_eq}$. As in the previous case, we cannot quantify the impact of this process in our study.

4.1.2.3. Transpiration of Trees

The transpiration of leaves produces additional moisture in the atmosphere that can also deviate the isotopic composition of water vapor from the isotopic equilibrium with rain. Trees take up soil water by their roots without isotopic fractionation (Bariac et al., 1990; Dawson & Ehleringer, 1993; Rothfuss & Javaux, 2017) although there is growing evidence that root water uptake fractionates water for deuterium (see, e.g., the recent study done by Barbeta et al., 2019, and references herein). The water ascends into the trunk in the xylem network without isotopic fractionation (Förstel & Hützen, 1983; Gessler et al., 2014; White et al., 1985). It then reaches the leaves where transpiration takes place. This evaporative process induces an isotopic enrichment of leaf water (Gonfiantini et al., 1965). It is often assumed that the $\delta^{18}O$ of transpired water vapor is equal to that of plant source water. This assumption about transpiration, occurring at isotopic steady state, is valid at daily or longer time scales (Cuntz et al., 2007). The isotopic composition of leaf water and water flux has a diurnal cycle controlled by rh (Cernusak et al., 2016). The daily enrichment maximum is reached at the beginning of afternoon when rh is the lowest. Then, the enrichment decreases gradually throughout the afternoon and night until reaching a minimum at the beginning of the morning. Since tree source water may be enriched compared to precipitation, transpiration of plants may lead to an enrichment of the vapor that could induce a positive $\Delta^{18}O_{vap\_eq}$.

As for soil evaporation, it is possible to quantify the contribution (x) of tree transpiration to the isotopic composition of near-surface water vapor by

$$\delta_{vap} = x \times \delta_{transpiration} + (1-x) \times \delta_{vap\_eq} \quad (10)$$

So that x is equal to

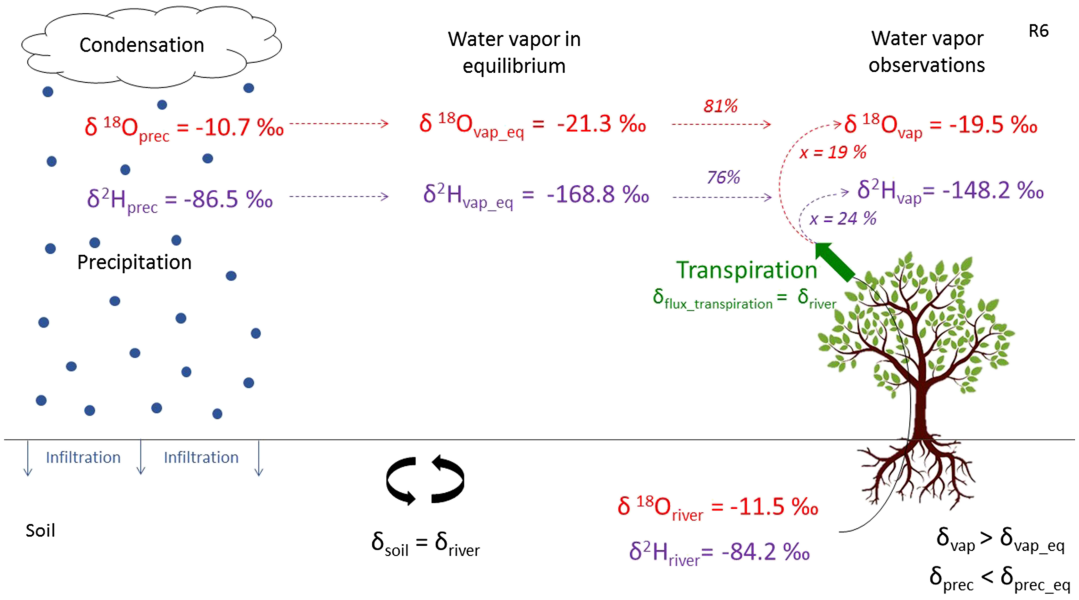

Figure 6. Diagram representing how transpiration from trees produces a departure from the isotopic equilibrium between precipitation and water vapor. This figure corresponds to the R6 event and $\delta^{18}O_{soil}$ is the mean isotopic composition of the river samples.

$$x = \left(\frac{\delta_{vap} - \delta_{vap\_eq}}{\delta_{transpiration} - \delta_{vap\_eq}}\right), \tag{11}$$

where $\delta_{transpiration}$ is equal to δ_{soil} that we take equal to the mean isotopic composition of the river samples (see section 4.1.1.2).

The values of x calculated with $\delta^{18}O$ and $\delta^{2}H$ are mutually consistent. The tree transpiration can explain the observed isotopic disequilibriums with a contribution of transpired vapor to atmospheric water vapor between 14% and 29% (Table 2 and Figure 6). However, if transpiration is responsible for liquid-vapor isotopic disequilibriums for R6 to R11 events, this process hardly accounts for the negative relationship between $\Delta^{18}O_{vap\_eq}$ and $\delta^{18}O_{prec}$.

4.1.3. Consequences for the Equilibrium Hypothesis Between Rain and Water Vapor Along the Growing Season

Between 27 February and 12 March 2017, the isotopic disequilibriums between precipitation and water vapor at the study site are small ($\Delta^{18}O_{vap\_eq}$ vary from −2.0‰ to 4.1‰, section 3). This may arise from high relative humidity at the site during the field campaign (between 70% and 96%) favoring isotopic exchanges between the water phases toward isotopic equilibrium. The observed $\Delta^{18}O_{vap\_eq}$ can be explained by several processes like tree transpiration or, for some cases, like droplets evaporation.

Each individual rain deviates from the isotopic equilibrium state with water vapor. However, the very significant relationship between the isotopic observations in water vapor and their expected values at equilibrium ($r^2 = 0.78$, $p < 0.01$) indicates that equilibrium prevails when considering a longer time scale (here 2 weeks). This suggests that the isotopic equilibrium is a more robust assumption at the subseasonal scale than for individual rain events, as already pointed out in previous studies (Deshpande et al., 2010; Lekshmy et al., 2018) and that the simplifying hypothesis of the isotopic equilibrium between water vapor and tree source water, which is often made in tree ring studies, can be well founded.

4.2. Consequences of the Isotopic Equilibrium Hypothesis on $\delta^{18}O_{cell}$ Calculation

At our site, the isotopic equilibrium between precipitation and water vapor appeared to be reached over a long period of time (2 weeks). Therefore, equilibrium can also be assumed to be achieved at the scale of the growing season and the mean value of $\delta^{18}O_{vap}$ measured during the monitoring period to be close to the mean value of $\delta^{18}O_{vap}$ over the whole growing season. Under these assumptions, we calculated the

Table 3
Variables Used in Section 4.2 and Comparison Between Observed and Calculated Isotopic Composition for the Water Source, Leaf Water, and Cellulose

Variable	Value	Origin
T_{air}	12.1 °C	Mean diurnal values over the monitoring period
rh	67%	Mean diurnal values over the monitoring period
$\delta^{18}O_{vap}$	−17.9‰	Mean diurnal values over the monitoring period
T_{leaf}	15.3 ± 0.8 °C	Calculated from T_{air} (equation 13)
ε_k	27.8 ± 0.1‰	Mean value in *Nothofagus*, calculated from data in Cernusak et al. (2016) (unpublished data from M. Barbour)
ε^*	10.1 ± 0.1‰	Calculated from T_{leaf} (equations (S11) and (S4) of Text S1)
w_a/w_i	0.5	Calculated with Buck's (1981) equation (equation (S7) of Text S1)
ε_{bio}	27.3 ± 0.2‰	Calculated from T_{leaf} (equation (S9) of Text S1)
p_{ex}	0.40 ± 0.02	Mean value (Sternberg & Ellsworth, 2011)
	Result	Measured parameters
$\delta^{18}O_{source}$	−7.9 ± 0.1‰	$\delta^{18}O_{river} = -11.5 \pm 0.5‰$ ($n = 10$); $\delta^{18}O_{weighted\ precipitation} = -9.7 \pm 3.7‰$ ($n = 11$)
$\delta^{18}O_{site}$	9.4 ± 1.0‰	$\delta^{18}O_{leaf} = 5.9 \pm 0.4‰$ ($n = 6$)
$\delta^{18}O_{cell}$	29.8 ± 0.7‰	$\delta^{18}O_{cell\text{-}mes} = 30.4 \pm 0.6‰$ ($n = 5$)

Note. Diurnal stands for the 8 a.m. to 8 p.m. time period.

isotopic composition of water at the evaporative sites in the leaves and in the current tree ring cellulose ($\delta^{18}O_{site}$ and $\delta^{18}O_{cell}$, respectively) assuming that source water is at the isotopic equilibrium with the mean isotopic composition of water vapor over the whole considered time period. We then compared whether the calculated $\delta^{18}O_{site}$ and $\delta^{18}O_{cell}$ are consistent with the measured isotopic values of the leaf water and of the cellulose synthetized by *Nothofagus* during the 2016–2017 growing season.

$\delta^{18}O_{source}$ was derived from $\delta^{18}O_{vap}$ following equation 2. $\delta^{18}O_{site}$ was calculated from the isotopic enrichment at the evaporative sites (e.g., Cernusak et al., 2016; details in Text S1) as follows:

$$\delta^{18}O_{site} = \Delta_{site} + \left(\frac{\delta^{18}O_{source} \times \Delta_{site}}{1000}\right) + \delta^{18}O_{source} \tag{12}$$

With Δ_{site}, the isotopic enrichment of water at evaporative site compared to source water, given by (Farquhar et al., 2007):

$$\Delta_{site} = \left(1 + \varepsilon^*\right) \times \left[\left(1 + \varepsilon_k\right) \times \left(1 - \frac{w_a}{w_i}\right) + \frac{w_a}{w_i}\left(1 + \Delta_{vap}\right)\right] - 1, \tag{13}$$

where ε^* is defined as

$$\varepsilon^* = \left(\alpha_{eq} - 1\right) \tag{14}$$

The ε_k is the kinetic fractionation for combined diffusion through the stomata and the boundary layer, w_a is the water vapor mole fraction in the atmosphere, w_i is the water vapor mole fraction in the intercellular air spaces inside leaves, and Δ_{vap} is the isotopic enrichment of atmospheric water vapor compared to source water.

$\delta^{18}O_{cell}$ was estimated using the model proposed by Sternberg et al. (1986), Yakir and DeNiro (1990), and Luo and Sternberg (1992), which takes into account additional oxygen exchange between sugars and xylem water during cellulose biosynthesis (see also Text S1):

$$\delta^{18}O_{cell} = p_{ex} \times \left(\delta^{18}O_{source} + \varepsilon_{bio}\right) + \left(1 - p_{ex}\right) \times \left(\delta^{18}O_{site} + \varepsilon_{bio}\right) \tag{15}$$

Where p_{ex} is the fraction of oxygen from sugars that undergoes exchange with xylem water, and ε_{bio} is the mean isotopic biochemical fractionation factor.

The values of the various variables used in the calculations are reported in Table 3. Air temperature, relative humidity, and the isotopic composition of water vapor were averaged over the daytime (8 a.m. to 8 p.m.) of the monitoring period when cellulose is expected to be formed. The leaf temperature (T_{leaf}) was estimated from regression analysis of measured T_{leaf} versus measured T_{air} using a $T_{leaf} - T_{air}$ database acquired for *Nothofagus* leaves (Cernusak et al., 2016):

$$T_{leaf} = 1.08 \pm 0.05 \times T_{air} + 2.26 \pm 1.20 \quad \text{with } r^2 = 0.95\ (n = 24) \tag{16}$$

The proportion of oxygen atoms exchanging with medium water during cellulose biosynthesis was considered to be $p_{ex} = 0.40 \pm 0.02$. Although, this variable can vary in a wide range, from 0.29 and 0.77 (Cheesman & Cernusak, 2016; Luo & Sternberg, 1992; Sternberg et al., 2006), the majority of p_{ex} estimations is close to 40% (Gessler et al., 2014).

The values calculated for $\delta^{18}O_{source}$, $\delta^{18}O_{site}$, and $\delta^{18}O_{cell}$ are -7.9 ± 0.1‰, 9.4 ± 1‰, and 29.8 ± 0.7‰, respectively. They are reported in Table 3, along with the mean value of the observed isotopic composition of rivers and springs, the mean amount-weighted $\delta^{18}O_{prec}$, and the mean value of $\delta^{18}O_{Cell}$ of the ring formed during the 2016–2017 growing season.

The source water for the tree is the xylem water, which is similar to the soil water, which in turn derives from precipitation. Here, the isotopic composition values for the rivers (measured $\delta^{18}O_{river}$) are lower than the one of the xylem water (calculated $\delta^{18}O_{source}$). This result is not surprising as precipitation from higher elevation and possibly melt water from snowpack at the top of the Perito Moreno range may contribute to the river water while the xylem water derives from the local precipitation. The isotopic difference between xylem and precipitation (measured $\delta^{18}O_{prec}$) may result from mixing and evaporation, taking place in the soil, which can lead to an isotopic enrichment of the water soil at the depth tapped by trees. By assuming that seasonal $\delta^{18}O_{prec}$ cycle follows the seasonal temperature cycle (as observed in the closest Chilean International Atomic Energy Agency station, Coyhaique, 45°35′S; 75°07′W), an artificial $\delta^{18}O_{prec}$ seasonal cycle based on Pampa Linda temperature in 2017, a March 2017 $\delta^{18}O_{prec}$ value of −9.7‰ (mean $\delta^{18}O_{prec}$ over our rain events) and an isotopic gradient of 0.5‰/°C can be estimated. The amount-weighted average $\delta^{18}O_{prec}$, inferred from the artificial isotopic seasonal cycle and Pampa Linda precipitation amount, is -8.9 ± 1.1‰ from November to April. The calculated $\delta^{18}O_{source}$ of −7.9‰ is thus consistent with an evaporation of the averaged rain over the growing period of the trees. Let us note that this calculation is based on the hypothesis that seasonal $\delta^{18}O_{prec}$ is fully controlled by temperature which may be oversimplified.

The isotopic composition at the evaporative site (calculated $\delta^{18}O_{site}$) is 4.5‰ higher than the measured leaves water (measured $\delta^{18}O_{leaf}$ of 5.9‰). Bulk leaf water is a mixing between unfractionated source water and enriched water at the evaporative sites (Cernusak et al., 2016; Holloway-Phillips et al., 2016, and references herein). Therefore, its oxygen isotopic composition is expected to be lower than $\delta^{18}O_{site}$. The portion that represents the unfractionated pool is often calculated to be 20% to 30% of the total water volume of a leaf (Flanagan et al., 1991). Here, according to a simple mass balance calculation, the unfractionated water is 20% of the total water volume of the leaf. Our results are thus consistent with previous estimations.

The calculated $\delta^{18}O_{cell}$ matches the one measured for the 2016–2017 ring. This result supports the hypothesis of water vapor and source water at the isotopic equilibrium over the growing tree period. However, it is worth noting that important hypotheses and simplification are done in our calculation, which encourages cautions regarding the interpretation of the results:

- Our leaf sampling being restricted to six leaves, collected at the same time (between 15:30 and 16:30) on the same day (25 March), the measured $\delta^{18}O_{leaf}$ may not be representative of the leaves water isotopic composition at the site-scale over the whole growing season.
- The values of $\delta^{18}O_{site}$ and $\delta^{18}O_{cell}$ being very sensitive to T_{leaf}, and even more to the difference between T_{air} and T_{leaf} (which affects w_i/w_a), an inaccurate appraisal of T_{leaf} may lead to significant errors on the final estimations. Direct measurements of T_{leaf} would strengthen the demonstration by removing some uncertainties.
- The monitoring period being restricted to a month at the end of the growing season, the environmental parameters we have measured may not be fully representative of the whole growing season, while the

cellulose of the ring 2016–2017 integrates the entire period. In our calculations, we considered the mean temperature between 8 a.m. and 8 p.m. over the monitoring period. To test if this period was representative of the growing period, we also calculated the mean temperature in Pampa Linda between 8 a.m. and 8 p.m. over the entire growing season (November to April). At Pampa Linda, the growing season temperature is 1 °C higher than the one corresponding to the monitoring period. Assuming that the difference of temperature between growing and monitoring periods is the same at our study site, we calculate $\delta^{18}O_{cell}$ if the temperature was 1 °C higher ($T_{air} + 1 = 13.1$ °C) and obtain a value of 29.5‰, that is a difference of −0.3‰ with the $\delta^{18}O_{cell}$ calculated with the temperature of the monitoring period. This difference is negligible for our discussion.

- Finally, the model used for $\delta^{18}O_{site}$ and $\delta^{18}O_{cell}$ calculation is a simple version which does not include nonsteady state and Péclet effects (as in Cuntz et al., 2007 and Ogée et al., 2009, for instance). Let us note, however, that the oxygen isotope composition of tree ring cellulose is not sensitive to the value of the Péclet effective length and that a simple two-pool model (enriched pool at the evaporative sites and xylem) can be adequate (Ogée et al., 2009).

Due to these uncertainties and estimates, the concordance between measured and calculated $\delta^{18}O_{cell}$ under the hypothesis of the isotopic equilibrium between source water and water vapor may be somewhat fortuitous. Indeed, there is little reason why the isotopic equilibrium between water vapor and soil water should be achieved except if the soil water is the unmodified accumulation of precipitation. The composition of soil water maybe a several-month integrator of weighted mean rainfall input modified, to some extent, by selective recharge, mixing and fractionation processes. It may be very different from the accumulated unfractionated meteoric water during the growing season. Actually, this hypothesis is based on the isotopic equilibrium between two isotopic variables that have different time variabilities ($\delta^{18}O_{vap}$ varies at subhourly scale, as shown by our measurements, whereas $\delta^{18}O_{source}$ has a longer period of variability which depends on the residence time of the water in the soil). In addition, as shown in this paper, the rainfall and the water vapor may not even be in equilibrium, at the event scale at least. So, even if the results of our calculation under the hypothesis of the vapor-source equilibrium are in perfect agreement with the measured values, due to the uncertainties mentioned above, we strongly encourage new experiments, including T_{air}, rh, $\delta^{18}O_{vap}$ monitoring, soil and/or xylem water measurements, and leaf temperature measurements all along the growing tree season in order to clarify the vapor-source water equilibrium issue and strengthen the conceptual approach.

5. Conclusion

This paper deals with the isotopic disequilibrium between precipitation and water vapor in Patagonia, Argentina. Based on rain and water vapor isotopic observations, from 24 February to 26 March 2017, it explores how isotopic disequilibrium affects the estimations of the isotopic composition in tree ring cellulose, which assumes the isotopic equilibrium state between the two water phases.

Following 11 rain events, precipitation and water vapor are found close to the isotopic equilibrium (disequilibriums vary from −2.0‰ to 4.1‰). Several processes such as evaporation of droplets, water vapor condensation at high elevation, droplets size, and vegetation transpiration can be invoked to explain the deviation from the isotopic equilibrium. It is worth noting that we explore each process separately whereas they can act together.

The generally accepted assumption that precipitation and water vapor are in isotopic equilibrium is not fully reached in our site at the individual rain event scale between 24 February and 26 March 2017. However, on average, the isotopic equilibrium between water vapor and precipitation can be considered as a valid approximation since the covariation between the isotopic composition of water vapor and the one in equilibrium with precipitation is highly significant ($r^2 = 0.78$). It would be necessary to check whether the isotopic equilibrium assumption is valid or not over the whole period during which the source water used by trees is formed. Indeed, vegetation studies aiming at calculating $\delta^{18}O_{cell}$ assume that the isotopic composition of water vapor is in equilibrium with the source water. First, we show in our study that $\delta^{18}O_{vap}$ varies at daily and intraseasonal time scales whereas $\delta^{18}O_{source}$ varies very likely on longer time scale. As a consequence, we claim that the use of the isotopic equilibrium between water vapor and source is wrong if the source is supposed to be an integrated precipitation. In addition,

we show that we are able to calculate a correct $\delta^{18}O_{cell}$ provided that the $\delta^{18}O_{source}$ has a value higher than that of the precipitation over the growing season, that is to say imprinted by evaporation. At this point, it is difficult to propose a mechanism explaining a continuous equilibrium between water vapor and source.

At last, our study deals with only a few samples of soil water and leaf water and does not include measurements of xylem water samples. This leads to a rough comparison between the modeled isotopic composition of cellulose and the measured one since the composition of the source water is not precisely known. Our results encourage additional comprehensive studies including a large panel of necessary samples.

Acknowledgments
We thank Monique Pierre for extracting water from leaves, Amaelle Landais for performing the fluorination procedure, and Bénédicte Minster for analyzing the isotopic composition of water samples. We also thank two anonymous reviewers for their constructive comments. The sampling campaign was funded by the LEFE (Les Enveloppes Fluides et l'Environnement) French national program (IVAPAPA project) and the analyses by the BNP-Paribas Climate Initiative (THEMES project). All data are available on the PANGAEA® Data publisher (https://pangaea.de).

References

Alexandre, A., Landais, A., Vallet-Coulomb, C., Piel, C., Devidal, S., Pauchet, S., et al. (2018). The triple oxygen isotope composition of phytoliths as a proxy of continental atmospheric humidity: Insights from climate chamber and climate transect calibrations. *Biogeosciences*, *15*(10), 3223–3241. https://doi.org/10.5194/bg-15-3223-2018

Aravena, J. C., LAra, A., Wolodarsky-Franke, A., Villalba, R., & Cuq, E. (2002). Tree-ring growth patterns and temperature reconstruction from Nothofagus pumilio (Fagaceae) forests at the upper tree line of southern Chilean Patagonia Tree-ring growth patterns and temperature reconstruction from Nothofagus pumilio (Fagaceae) forest. *Revista Chilena de Historia Natural*, *75*, 361–376. https://doi.org/10.4067/S0716-078X2002000200008

Arco Molina, J. G., Helle, G., Hadad, M. A., & A., R. F. (2019). Variations in the intrinsic water-use efficiency of north Patagonian forests under a present climate change scenario: Tree age, site conditions and long-term environmental effects. *Tree Physiology*, *00*, 1–18. https://doi.org/10.1093/treephys/tpy144

Barbeta, A., Jones, S. P., Clavé, L., Wingate, L., Gimeno, T. E., Fréjaville, B., et al. (2019). Unexplained hydrogen isotope offsets complicate the identification and quantification of tree water sources in a riparian forest. *Hydrology and Earth System Sciences*, *23*, 2129–2146. https://doi.org/10.5194/hess-23-2129-2019

Bariac, T., Klamecki, A., Jusserand, C., & Létolle, R. (1990). Evolution de la composition isotopique de l'eau (^{18}O) dans le continuum sol-plante-atmosphere. *Geochimica et Cosmochimica Acta*, *54*, 413–424. https://doi.org/10.1016/S0341-8162(87)80006-1

Barkan, E., & Luz, B. (2005). High precision measurements of $^{17}O/^{16}O$ and $^{18}O/^{16}O$ ratios in H_2O. *Rapid Communications in Mass Spectrometry*, *19*(24), 3737–3742. https://doi.org/10.1002/rcm.2250

Barnes, C. J., & Allison, G. B. (1983). The distribution of deuterium and ^{18}O in dry soils, 1. *Theory. Journal of Hydrology*, *60*, 141–156. https://doi.org/10.1016/0022-1694(83)90078-1

Barnes, C. J., & Allison, G. B. (1984). The distribution of deuterium and ^{18}O in dry soils, 3. *Theory for non-isothermal water movement. Journal of Hydrology*, *74*, 119–135. https://doi.org/10.1016/0022-1694(83)90018-5

Barnes, C. J., & Allison, G. B. (1988). Tracing of water movement in the unsaturated zone using stable isotopes of hydrogen and oxygen. *Journal of Hydrology*, *100*, 143–176. https://doi.org/10.1016/0022-1694(84)90144-6

Boninsegna, J. A., Argollo, J., Aravena, J. C., Barichivich, J., Christie, D., Ferrero, M. E., et al. (2009). Dendroclimatological reconstructions in South America: A review. *Palaeogeography, Palaeoclimatology, Palaeoecology*, *281*(3–4), 210–228. https://doi.org/10.1016/j.palaeo.2009.07.020

Bony, S., Risi, C., & Vimeux, F. (2008). Influence of convective processes on the isotopic composition ($\delta^{18}O$ and δD) of precipitation and water vapor in the tropics: 1. Radiative-convective equilibrium and Tropical Ocean-Global Atmosphere-Coupled Ocean-Atmosphere Response Experiment (TOGA-COARE). *Journal of Geophysical Research: Atmosphere*, *113*(19), 1–21. https://doi.org/10.1029/2008JD009942

Braud, I., Bariac, T., Biron, P., & Vauclin, M. (2009). Isotopic composition of bare soil evaporated water vapor. Part II: Modeling of RUBIC IV experimental results. *Journal of Hydrology*, *369*(1–2), 17–29. https://doi.org/10.1016/j.jhydrol.2009.01.038

Braud, I., Biron, P., Bariac, T., Richard, P., Canale, L., Gaudet, J.-P., & Vauclin, M. (2009). Isotopic composition of bare soil evaporated water vapor. Part I: RUBIC IV experimental setup and results. *Journal of Hydrology*, *369*(1–2), 1–16. https://doi.org/10.1016/j.jhydrol.2009.01.034

Braud, I., Bariac, T., Gaudet, J. P., & Vauclin, M. (2005). SiSPAT-Isotope, a coupled heat, water and stable isotope (HDO and H_2O^{18}) transport model for bare soil. Part I. Model description and first verifications. *Journal of Hydrology*, *309*, 277–300. https://doi.org/10.1016/j.jhydrol.2004.12.013

Braud, I., Bariac, T., Vauclin, M., Boujamlaoui, Z., Gaudet, J. P., Biron, P., & Richard, P. (2005). SiSPAT-Isotope, a coupled heat, water and stable isotope (HDO and H_2O^{18}) transport model for bare soil. Part II. Evaluation and sensitivity tests using two laboratory data sets. *Journal of Hydrology*, *309*, 301–320. https://doi.org/10.1016/j.jhydrol.2004.12.012

Brutsaert, W. (1982). *Evaporation into the atmosphere*. (Springer, Ed.) (1st ed. 19). Springer Netherlands. https://doi.org/10.1007/978-94-017-1497-6

Buck, A. L. (1981). New equations for computing vapor pressure and enhancement factor. *Journal of Applied Meteorology*, *20*, 1527–1532. https://doi.org/10.1175/1520-0450(1981)020%3C1527:NEFCVP%3E2.0.CO;2

Cernusak, L. A., Barbour, M. M., Arndt, S. K., Cheesman, A. W., English, N. B., Feild, T. S., et al. (2016). Stable isotopes in leaf water of terrestrial plants. *Plant Cell and Environment*, *39*(5), 1087–1102. https://doi.org/10.1111/pce.12703

Cheesman, A. W., & Cernusak, L. A. (2016). In fidelity in the outback: Climate signal recorded in $\Delta^{18}O$ of leaf but not branch cellulose of eucalypts across an Australian aridity gradient. *Tree Physiology*, *37*, 554–564. https://doi.org/10.1093/treephys/tpw121

Craig, H., & Gordon, L. I. (1965). Deuterium and oxygen 18 variations in the ocean and the marine atmosphere. *Stable Isotopes in Oceanographic Studies and Paleotemperatures*, 9–130.

Cuntz, M., Ogée, J., Farquhar, G. D., Peylin, P., & Cernusak, L. A. (2007). Modelling advection and diffusion of water isotopologues in leaves. *Plant, Cell and Environment*, *30*(8), 892–909. https://doi.org/10.1111/j.1365-3040.2007.01676.x

Dansgaard, W. (1964). Stable isotopes in precipitation. *Tellus*, *16*(4), 436–468. https://doi.org/10.3402/tellusa.v16i4.8993

Darling, W. G. (2004). Hydrological factors in the interpretation of stable isotopic proxy data present and past: A European perspective. *Quaternary Science Reviews*, *23*, 743–770. https://doi.org/10.1016/j.quascirev.2003.06.016

Dawson, T. E., & Ehleringer, J. R. (1993). Isotopic enrichment of water in the "woody" tissues of plants: Implications for plant water source, water uptake, and other studies which use the stable isotopic composition of cellulose. *Geochimica et Cosmochimica Acta*, *57*, 3487–3492. https://doi.org/10.1016/0016-7037(93)90554-A

Deshpande, R. D., Maurya, A. S., Kumar, B., Sarkar, A., & Gupta, S. K. (2010). Rain-vapor interaction and vapor source identification using stable isotopes from semiarid western India. *Journal of Geophysical Research: Atmosphere*, *115*(23), 1–11. https://doi.org/10.1029/2010JD014458

Dongmann, G., Nürnberg, H. W., Förstel, H., & Wagener, K. (1974). On the enrichment of $H_2^{18}O$ in the leaves of transpiring plants. *Radiation and Environmental Biophysics*, *11*(1), 41–52. https://doi.org/10.1007/BF01323099

Farquhar, G. D., Cernusak, L. A., & Barnes, B. (2007). Heavy water fractionation during transpiration. *Plant Physiology*, *143*, 11–18. https://doi.org/10.1104/pp.106.093278

Flanagan, L. B., Comstock, J. P., & Ehieringer, J. R. (1991). Comparison of modeled and observed environmental influences on the stable oxygen and hydrogen isotope composition of leaf water in *Phaseolus vulgaris* L. *Plant Physiology*, *96*, 588–596. https://doi.org/10.1104/pp.96.2.588

Förstel, H., & Hützen, H. (1983). Oxygen isotope ratios in German groundwater. *Nature*, *304*(18), 614–616. https://doi.org/10.1038/304614a0

Garreaud, R. D., Lopez, P., Minvielle, M., & Rojas, M. (2013). Large-scale control on the Patagonian climate. *Journal of Climate*, *26*, 215–231. https://doi.org/10.1175/JCLI-D-12-00001.1

Gessler, A., Ferrio, J. P., Hommel, R., Treydte, K., Werner, R. A., & Monson, R. K. (2014). Stable isotopes in tree rings: Toward a mechanistic understanding of isotope fractionation and mixing processes from the leaves to the wood. *Tree Physiology*, *34*(8), 796–818. https://doi.org/10.1093/treephys/tpu040

Gonfiantini, R., Gratziu, S., & Tongiorgi, E. (1965). Oxygen isotopic composition of water in leaves. *Isotopes and Radiation in Soil-Plant Nutrition Studies*, 405–410.

Grießinger, J., Langhamer, L., Schneider, C., Saß, B. L., Steger, D., Skvarca, P., et al. (2018). Imprints of climate signals in a 204 year $\delta^{18}O$ tree-ring record of *Nothofagus pumilio* from Perito Moreno Glacier, Southern Patagonia (50°S). *Frontiers in Earth Science*, *6*, 1–17. https://doi.org/10.3389/feart.2018.00027

Halder, J., Terzer, S., Wassenaar, L. I., Araguas-Araguas, L. I., & Aggarwal, P. K. (2015). The Global Network of Isotopes in Rivers (GNIR): Integration of water isotopes in watershed observation and riverine research. *Hydrology and Earth System Sciences*, *19*, 3419–3431. https://doi.org/10.5194/hess-19-3419-2015

Han, L.-F., Gröning, M., Aggarwal, P., & Helliker, B. R. (2006). Reliable determination of oxygen and hydrogen isotope ratios in atmospheric water vapour adsorbed on 3A molecular sieve. *Radiation and Environmental Biophysics*, *20*, 3612–3618. https://doi.org/10.1002/rcm

Holloway-Phillips, M., Cernusak, L. A., Barbour, M., Song, X., Cheesman, A., Munksgaard, N., et al. (2016). Leaf vein fraction influences the Péclet effect and ^{18}O enrichment in leaf water. *Plant Cell and Environment*, *14*, 2414–2427. https://doi.org/10.1111/pce.12792

Lara, A., Wolodarsky-Franke, A., Aravena, J. C., Villalba, R., Solari, M. E., Pezoa, L., et al. (2005). Climate fluctuations derived from tree-rings and other proxy-records in the Chilean Andes: State of the art and future prospects. *Advances in Global Change Research*, *23*(January), 145–156. https://doi.org/10.1007/1-4020-3508-X

Lavergne, A., Daux, V., Pierre, M., Stievenard, M., Srur, A., & Villalba, R. (2018). Past summer temperatures inferred from dendrochronological records of *Fitzroya cupressoides* on the eastern slope of the Northern Patagonian Andes. *Journal of Geophysical Research: Biogeosciences*. https://doi.org/10.1002/2017JG003989

Lavergne, A., Daux, V., Villalba, R., Pierre, M., Stievenard, M., & Srur, A. M. (2017). Improvement of isotope-based climate reconstructions in Patagonia through a better understanding of climate influences on isotopic fractionation in tree rings. *Earth and Planetary Science Letters*, *1*, 1–9. https://doi.org/10.1016/j.epsl.2016.11.045

Lavergne, A., Daux, V., Villalba, R., Pierre, M., Stievenard, M., Srur, A. M., & Vimeux, F. (2016). Are the $\delta^{18}O$ of *F. cupressoides* and *N. pumilio* promising proxies for climate reconstructions in northern Patagonia? *Journal of Geophysical Research: Biogeosciences*, *121*(3), 767–776. https://doi.org/10.1002/2015JG003260

Leavitt, S. W., & Danzer, S. R. (1993). Method for batch processing small wood samples to holocellulose for stable-carbon isotope analysis. *Analytical Chemistry*, *65*, 87–89. https://doi.org/10.1021/ac00049a017

Lekshmy, P. R., Midhun, M., & Ramesh, R. (2018). Influence of stratiform clouds on δD and $\delta^{18}O$ of monsoon water vapour and rain at two tropical coastal stations. *Journal of Hydrology*, *563*, 354–362. https://doi.org/10.1016/j.jhydrol.2018.06.001

Luo, Y. H., & Sternberg, L. D. S. L. (1992). Hydrogen and oxygen isotopic fractionation during heterotrophic cellulose synthesis. *Journal of Experimental Botany*, *43*(246), 47–50. https://doi.org/10.1093/jxb/43.1.47

Majoube, M. (1971). Fractionnement en oxygène 18 et en deutérium entre l'eau et sa vapeur. *Journal de Chimie et Physique*, *68*, 1423–1436. https://doi.org/10.1051/jcp/1971681423

Mathieu, R., & Bariac, T. (1996). A numerical model for the simulation of stable isotope profiles in drying soils. *Journal of Geophysical Research*, *101*(D7), 12685–12696. https://doi.org/10.1029/96JD00223

Merlivat, L. (1978). Molecular diffusivities of H_2O^{16}, HDO^{16}, and H_2O^{18} in gases. *The Journal of Chemical Physics*, *69*(6), 2864–2871. https://doi.org/10.1063/1.436884

Mundo, I. A., Jun, F. A. R., Villalba, R., Kitzberger, T., & Barrera, M. D. (2012). *Araucaria araucana* tree-ring chronologies in Argentina: Spatial growth variations and climate influences. *Trees*, *26*, 443–458. https://doi.org/10.1007/s00468-011-0605-3

Muñoz, A.A., Barichivich, J., Christie, D.A., Dorigo, W., Sauchyn, D., González-Reyes, Á., et al. (2013). Patterns and drivers of *Araucaria araucana* forest growth along a biophysical gradient in the northern Patagonian Andes: Linking tree rings with satellite observations of soil moisture. *Austral Ecology*, (January), 12 pp. https://doi.org/10.1111/aec.12054

Ogée, J., Barbour, M. M., Wingate, L., Bert, D., Bosc, A., Stievenard, M., et al. (2009). A single-substrate model to interpret intra-annual stable isotope signals in tree-ring cellulose. *Plant Cell and Environment*, *32*(8), 1071–1090. https://doi.org/10.1111/j.1365-3040.2009.01989.x

Roig, F. A., Siegwolf, R., & Boninsegna, J. A. (2006). Stable oxygen isotopes (δ18O) in *Austrocedrus chilensis* tree rings reflect climate variability in northwestern Patagonia, Argentina. *International Journal of Biometeorology*, *51*, 97–105. https://doi.org/10.1007/s00484-006-0049-4

Rothfuss, Y., & Javaux, M. (2017). Reviews and syntheses: Isotopic approaches to quantify root water uptake: A review and comparison of methods. *Biogeosciences*, *14*, 2199–2224. https://doi.org/10.5194/bg-14-2199-2017

Rothfuss, Y., Merz, S., Vanderborght, J., Hermes, N., Weuthen, A., Pohlmeier, A., et al. (2015). Long-term and high-frequency non-destructive monitoring of water stable isotope profiles in an evaporating soil column. *Hydrology and Earth System Sciences*, *19*, 4067–4080. https://doi.org/10.5194/hess-19-4067-2015

Saylor, J. E., Moras, A., Horton, B. K., & Nie, J. (2009). Controls on the isotopic composition of surface water and precipitation in the Northern Andes, Colombian Eastern Cordillera. *Geochimica et Cosmochimica Acta*, *73*, 6999–7018. https://doi.org/10.1016/j.gca.2009.08.030

Seluchi, M. E., Saulo, A. C., Nicolini, M., & Satyamurty, P. (2003). The northwestern Argentinean low: A study of two typical events. *Monthly Weather Review*, *131*(10), 2361–2378. https://doi.org/10.1175/1520-0493(2003)131<2361:TNALAS>2.0.CO;2

Sprenger, M., Leistert, H., Gimbel, K., & Weiler, M. (2016). Illuminating hydrological processes at the soil-vegetation- atmosphere interface with water stable isotopes. *Reviews of Geophysics*, *54*, 674–704. https://doi.org/10.1002/2015RG000515

Sternberg, L., Deniro, M. J., & Savidge, R. A. (1986). Oxygen isotope exchange between metabolites and water during biochemical reactions leading to cellulose synthesis. *Plant Physiology*, *82*(2), 423–427. https://doi.org/10.1104/pp.82.2.423

Sternberg, L., & Ellsworth, P. F. V. (2011). Divergent biochemical fractionation, not convergent temperature, explains cellulose oxygen isotope enrichment across latitudes. *PLoS ONE*, *6*(11), 1–7. https://doi.org/10.1371/journal.pone.0028040

Sternberg, L., Pinzon, M. C., Anderson, W. T., & Jahren, A. H. (2006). Variation in oxygen isotope fractionation during cellulose synthesis: Intramolecular and biosynthetic effects. *Plant Cell and Environment*, *29*, 1881–1889. https://doi.org/10.1111/j.1365-3040.2006.01564.x

Sternberg, L. (2009). Oxygen stable isotope ratios of tree-ring cellulose: The next phase of understanding. *New Phytologist*, *181*, 553–562. https://doi.org/10.1111/j.1469‐8137.2008.02661.x

Stewart, M. K. (1975). Stable isotope fractionation due to evaporation and isotopic exchange of falling water drops. *Journal of Geophysical Research*, *80*(9), 1133–1146. https://doi.org/10.1029/JC080i009p01133

Tognetti, R., Lombardi, F., Lasserre, B., Cherubini, P., & Marchetti, M. (2014). Tree-ring stable isotopes reveal twentieth-century increases in water-use efficiency of *Fagus sylvatica* and *Nothofagus* spp. in Italian and Chilean mountains. *PLoS ONE*, *9*(11), 1–16. https://doi.org/10.1371/journal.pone.0113136

Tremoy, G., Vimeux, F., Cattani, O., Mayaki, S., Souley, I., & Favreau, G. (2011). Measurements of water vapor isotope ratios with wavelength- scanned cavity ring-down spectroscopy technology: New insights and important caveats for deuterium excess measurements in tropical areas in comparison with isotope-ratio mass spectrometry. *Rapid Communications in Mass Spectrometry*, *25*(July), 3469–3480. https://doi.org/10.1002/rcm.5252

Tremoy, G., Vimeux, F., Soumana, S., Souley, I., Risi, C., Favreau, G., & Oi, M. (2014). Clustering mesoscale convective systems with laser-based water vapor $\delta^{18}O$ monitoring in Niamey (Niger). *Journal of Geophysical Research: Atmosphere*, *119*, 1–25. https://doi.org/10.1002/2013JD020968

Urrutia-Jalabert, R., Malhi, Y., Barichivich, J., Lara, A., Delgado-Huertas, A., Rodríguez, C. G., & Cuq, E. (2015). Increased water use efficiency but contrasting tree growth patterns in *Fitzroya cupressoides* forests of southern Chile during recent decades. *Journal of Geophysical Research: Biogeosciences*, *120*, 2505–2524. https://doi.org/10.1002/2015JG003098

Villalba, R., Boninsegna, J. A., Veblen, T. T., Schmelter, A., & Rubulis, S. (1997). Recent trends in tree-ring records from high elevation sites in the Andes of Northern Patagonia. *Climatic Change*, *36*, 425–454. https://doi.org/10.1023/A

White, J. W. C., Cook, E. R., Lawrence, J. R., & Broecker, W. S. (1985). The D / H ratios of sap in trees: Implications for water sources and tree ring D/H ratios. *Geochimica et Cosmochimica Acta*, *49*, 237–246. https://doi.org/10.1016/0016-7037(85)90207-8

Yakir, D., & DeNiro, M. J. (1990). Oxygen and hydrogen isotope fractionation during cellulose metabolism in *Lemna gibba* L. *Plant Physiology*, *93*(1), 325–332. https://doi.org/10.1104/pp.93.1.325